Materials Science and Engineering C 33(2013) 864–869
DOI:http://dx.doi.org/10.1016/j.msec.2012.11.013

Effect of highly dispersed yttria addition on thermal stability of hydroxyapatite

P. Parente [a,*], B. Savoini [b], B. Ferrari [a], M.A. Monge [b], R. Pareja [b], A.J. Sanchez-Herencia [a]

[a] Instituto de Cerámica y Vidrio, CSIC, C/Kelsen 5, Madrid 28049, Spain
[b] Departamento de Física, Universidad Carlos III de Madrid, Avda. Universidad 30, Leganés 28911, Spain

Abstract: The capability of the colloidal method to produce yttria (Y_2O_3) dispersed hydroxyapatite (HA) has been in vestigated as an alternative method to the conventional method of mechanical mixing and sintering for de veloping HA based materials that could exhibit controllable and enhanced functional properties. A water based colloidal route to produce HA materials with highly dispersed Y_2O_3 has been applied, and the effect of 10 wt.% Y_2O_3 addition to HA investigated by thermal analysis, X ray diffraction and Fourier transform in frared spectroscopy. These measurements evidence a remarkable effect of this Y_2O_3 addition on decomposi tion mechanisms of synthetic HA. Results show that incorporation of Y_2O_3 as dispersed second phase is beneficial because it hinders the decomposition mechanisms of HA into calcium phosphates. This retardation will allow the control of the sintering conditions for developing HA implants with improved properties. Be sides, substitution of Ca^{2+} with Y^{3+} ions appears to promote the formation of OH^- vacancies, which could improve the conductive properties of HA favorable to osseointegration.

Keywords: Hydroxyapatite composite, Yttria, Free form fabrication , Thermal stability , FTIR

1. Introduction

The thermal stability of hydroxyapatite (HA), $Ca_{10}(PO_4)_6(OH)_2$, is a major concern for fabricating HA implants and coatings because the thermal decomposition on their processing modifies the prop erties of the HA materials, in particular the biomedical ones [1,2]. The decomposition of HA on heating proceeds in two stages: (1) partial dehydration yielding oxyhydroxyapatite (OHA) and water, i.e. $Ca_{10}(PO_4)_6(OH)_{2(1-x)}O_x\square_x + xH_2O$ ($\square$ denotes noncharged va cancies), followed by complete dehydroxylation that transforms OHA into oxyapatite (OA), $Ca_{10}(PO_4)_6O\square$, which is unstable and quickly rehydrates to OHA in air [1,3], and (2) subsequent irrevers ible decomposition of OHA along with HA in calcium phosphates [1,2,4 6]. The works reported about the thermal behavior of HA are mostly focused on the second stage, because it has a strong effect on the mechanical properties [2,7], chemical activity [8] and stability of HA within living organisms [9]. In contrast, the effect of dehydration on the properties of HA materials is often overlooked [2,4 6]. During the dehydration stage of HA, the progressive loss of hydroxyl groups in OHA can shift the temperature of the subsequent decomposition of OHA+HA into calcium phosphates drastically [1]. The study of decom position mechanisms is thus of key importance to optimize the process ing of HA materials.

Moreover, the bioactive HA ceramics for specific applications re quire certain degree of biodegradability and mechanical strength. It is known that these two characteristics are related with the porosity and presence of the tricalcium phosphate (TCP) phase, $Ca_3(PO_4)_2$ in the material [10]. Therefore, it would be interesting to investigate the characteristics of the decomposition and densification of HA for achieving control of the porosity and TCP content in the HA ceramics. The incorporation of substitutional cations in the crystal lattice of HA is also of considerable interest because it can modify the characteristics of the crystal lattice enhancing the thermal stability, the mechanical and conductive properties, and consequently the biological response of the HA implants [11 13].

The addition of yttria (Y_2O_3) to a bioactive glass ceramics and HA materials has been investigated in terms of physical, mechanical and biological properties [14 16]. Also, Y_2O_3 has been indirectly involved in biomedical applications. In particular, Y_2O_3 is the usual stabilizer of zirconia used in HA based composite materials and other biomedical applications [17 22]. It appears that the addition of Y_2O_3 improves mechanical properties of the HA materials maintaining a good biolog ical response. However, few papers reporting the effects of the Y_2O_3 addition on HA are found, and the comprehension of its effect on the properties of sintered HA materials is limited.

In the present work the effect of the nano sized yttria addition on the mechanisms of the HA decomposition during heating was investigated. Experiments of differential thermal analysis (DTA) and thermal gravi metric analysis (TGA), and measurements of X ray diffraction (XRD) and Fourier transform infrared (FTIR) spectroscopy, were performed to examine the changes that occur during heating of pure HA and HA 10 wt.% Y_2O_3 processed by an optimized colloidal route. This composition has been chosen because the decomposition and me chanical characteristics of a HA 10 wt.% Y_2O_3 material (named HA10Y hereafter) was previously investigated. In a study performed

E-mail address: pparente@icv.csic.es (P. Parente).

by Auger et al. [16], it was found that HA10Y, produced by dry me chanical mixing, cold isostatic pressing (CIP) and sintering, exhibited an enhanced thermal stability and somewhat better mechanical characteristics in comparison with the HA composites containing 10 wt.% of ZrO_2 or TiO_2.

It is hard to produce a homogeneous dispersion of nano sized par ticles in a solid matrix because the second phase particles tend to ag gregate during the processing of the starting powders. Nevertheless, it has been shown that the colloidal methods, like those described in Refs. [23 26], may be successful for obtaining this kind of disper sion in solid phase. Besides, the colloidal techniques allow the fabrica tion of ceramic parts with intricate shapes, and complex structures such as coatings, and layered or laminate materials. The high mobility of the particles in an appropriate colloidal suspension favors the ho mogeneous dispersion of phases of different nature in the precursor slurries of ceramic matrix composites that can be processed as porous or dense materials [27,28]. To accomplish a good dispersion of the starting powders is necessary to develop repulsive potentials between particles that prevent the particle agglomeration [26]. These repulsive potentials are achieved by adding to the particle suspension a dispersing agent that induces a surface charge in the particle. Several dispersants can be used depending on the specific application, the concentration of which has to be optimized for each particular case [29]. Thus, in the present work as prerequisite, the dispersion of Y_2O_3 particles in a HA10Y composite has had to be optimized looking for the appropriate amount of dispersing agent that has to be added to the suspension of HA Y_2O_3 to obtain the precursor colloid with better stability. This is determined from zeta potential measurements in colloidal suspensions of starting powders.

2. Materials and methods

Synthetic HA powder with a Ca/P ratio of 1.67 and mean particle size of 5 μm (Captal® 'S' HA, Plasma Biotal Ltd.) and nanosized Y_2O_3 with a primary particle size ranging between 15 and 30 nm (Nanophase Tech nologies) were used as starting materials. These powders have a specific surface area and a theoretical density of 1.5 $m^2\,g^{-1}$ and 3.1 $g\,cm^{-3}$ for HA, and of 60 $m^2\,g^{-1}$ and 4.5 $g\,cm^{-3}$ for Y_2O_3.

The zeta potential for these starting powders was determined by mi croelectrophoresis using a Zeta meter System 3.0+ (Zeta Meter Inc., USA) in the case of the HA suspensions, and by the laser Doppler velocimetry using a Zetasizer Nano ZS (Malvern, UK) for the Y_2O_3 sus pensions. The accurate determination of the zeta potential for the nano sized Y_2O_3 particles requires the measurement of the particle ve locity by laser Doppler velocimetry. The colloidal suspensions used for the measurements were prepared in a KCl 10^{-2} M water solution in order to maintain constant the ionic strength of the medium. For the present starting powders and measuring equipments, the optimum powder concentration in the suspensions resulted to be 0.1 $g\,cm^{-3}$. Polyacrylic acid (PAA) (Mw = 2,000, Acros Organics, USA), in an ammo nia solution with a molar ratio PAA/NH_3 of 1.5 for ensuring the PAA dis sociation, was used as anionic dispersant agent. Since the pH of the suspension has an effect on the zeta potential, their pH values were ad justed at pH = 10 using a dilute tetramethylammonium hydroxide solu tion (TMAH, Sigma Aldrich, Germany). The pH value of 10 was previously established elsewhere as the one that optimizes the colloidal processing of HA and Y_2O_3 starting powders [30]. A mean zeta potential from 10 measurements was obtained for each suspensions.

After determining in terms of wt.% the PAA content that optimizes the zeta potential, separated colloidal suspensions of HA and HA10Y containing a solid fraction of 45 vol.% in deionised and distilled water were prepared with their pH adjusted at 10, and with the optimum con centration of PAA dispersant previously determined for the HA and Y_2O_3 suspensions. The Ca/Y molar ratio in the HA10Y suspension is 10.1, that corresponds to $(10-y)/y$ with $y=0.9$, which is within the solubility limit ratio of ~2 for Y^{3+} in apatite [31]. These slurries were ball milled for 4 h to obtain a good dispersion of the Y_2O_3 particles in HA. A polyethylene container and Al_2O_3 balls were used. Then, the slur ries were slip cast on plaster of Paris molds and dried for 24 h in air to obtain porous green samples. These samples were sintered at 1250 °C for 90 min in air using heating and cooling rates of 5 °C min^{-1}.

The thermal behavior during sintering was studied by TGA DTA measurements over the temperature range 20 − 1450 °C at a heating rate of 5 °C min^{-1} using a thermal analyzer Netzsch STA 409. The den sities of the green and sintered samples were measured by the Archime des method using Hg, and the values were given as fraction of the theoretical density calculated applying the mix rule, i.e. 3.25 $g\,cm^{-3}$.

Microstructural and compositional analyses of the sintered samples were performed on polished sintered samples with a field emission scanning electron microscope (FE SEM Hitachi S 4700) equipped with energy dispersive X ray spectrometers (EDS). The samples were em bedded in an epoxy resin under vacuum to fill up the pores.

X ray diffraction (XRD) measurements were carried out in an X Pert Philips diffractometer using the Cu K_α radiation. The diffraction patterns were recorded through the range of 2θ angles between 10° and 100° in steps of 0.01°. The phases present in the sintered samples were identified from the quantitative analyses of the XRD patterns using the Rietveld method, the FULLPROF software, and the crystallographic data from the reference JCPDS files [32,33]. Lattice parameters of hexagonal structure were calculated using the reflections of the most intense peaks from HA and HA10Y XRD patterns.

The FTIR measurements were performed on sintered HA and HA10Y samples using a Perkin Elmer 2000 FTIR spectrometer to evaluate the optical absorption of the functional groups in the materials. The samples were ground using an agate mortar and pestle, and the powder was pressured thin on a KBr crystal. The spectra were acquired over the wave number range 4000 − 400 cm^{-1}, and the KBr contribution to the spectra subtracted.

3. Results and discussion

3.1. Material processing

The values of zeta potential of HA and Y_2O_3 measured as a function of the PAA concentration at pH 10 are reported in Fig. 1. It should be no ticed that the absolute values of zeta potential for HA are not compara ble with those for Y_2O_3 because the measurements were acquired with different instruments due to the differences in the particle size. Also, the measurements corresponding to HA have a higher error due to the re cording method of the experimental data. In any case, the sign and trend of the zeta potential give the information of interest about the be havior of both powders in aqueous suspension. The negative values of the zeta potential indicate that both surfaces of the HA and Y_2O_3

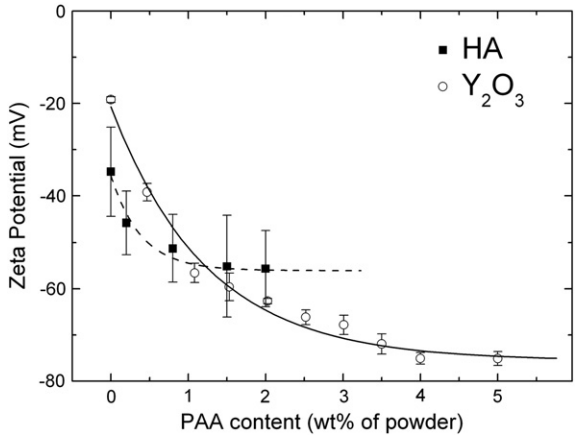

Fig 1. Zeta potential of HA and Y_2O_3 versus PAA concentration at pH = 10.

particles are negatively charged. Then, when both types of particles are in aqueous media, the mutual interaction will be repulsive avoiding ag glomeration and promoting the dispersion of Y_2O_3 in the HA10Y mate rial. It can be observed that zeta potential of HA powders decreases as the amount of dispersant increases up to a limit of 1 wt.%, which means that the surface of the particles is saturated of dispersant. Further PAA addition does not induce more negative values, and consequently any extra repulsion between the particles due to surface charges could not be expected. In the case of the nano sized Y_2O_3 particles, a disper sant fraction of 4 wt.% is required to achieve saturation. This higher frac tion was expected as the specific surface area of the Y_2O_3 particles is higher than the one for HA, and therefore a higher amount of dispersant can be adsorbed. According to the results, the slurries were prepared using dispersant amounts of $0.01 \times W_{HA}$ and $0.04 \times W_{YO}$, where W_{HA} and W_{YO} are the weights of HA and Y_2O_3 powders used for preparing the slurries.

3.2. Characterization of pure HA and HA10Y composite

3.2.1. Microstructural characterization

Measurements performed by Hg immersion provide apparent den sity measurements of the HA and HA10Y samples because this tech nique measures the apparent volume of the samples. Because of its high surface tension, Hg is a non wetting fluid with respect to air for solid materials, so it does not fill the pore space. Thus, porosity defined by the (total pore volume)/(apparent volume) ratio is given by [1 − (apparent density)/(theoretical density)]. The relative densities of the samples are summarized in Table 1. It should be observed that the HA density value is within the range of similar packed hydroxyapatite green bodies obtained by a similar method and with starting powders of the same particle size [25]. In the case of HA10Y, due to the difference in the particle sizes, a better packing is achieved and consequently a higher green density is measured. A sintering temperature of 1250 °C was selected to facilitate the formation of the neck and consolidation of a porous material. The sintering process affects the characteristics of the sintered materials in different ways. In the case of HA the density is higher in the sintered compact than in the green one, but still an ele vated amount of open and/or close pores remains. This indicates that the compaction of the HA sample under the present conditions took place at the intermediate stage of sintering, i.e. when grain boundary migration is activated, the particles join together and pore shrinkage is still proceeding. In contrast, for HA10Y a very slight increment in the density is observed indicating that Y_2O_3 particles could have de layed the sintering process by preventing the grain boundary migration. It should be mentioned that the densification degree achieved for HA10Y is very similar to the counterpart HA10Y material from Ref. [16], prepared by dry CIP and pressureless sintering.

Fig. 2 shows SEM images of the polished surfaces of sintered HA and HA10Y, and the fracture surface of HA10Y. Images (a) and (b) in Fig. 2 re veal that the present sintering conditions are appropriated for develop ing necks between HA particles, although a considerable micron sized interconnected pores resulting in open porosity is observed. These obser vations agree with the density measurements. In the case of the compos ite HA10Y, Fig. 2b shows Y_2O_3 particles with a mean size of about 200 nm completely surrounding the HA ones. This proves that a fine dis persion of Y_2O_3 particles has been achieved under the present processing conditions. In the micrograph of the fractured surface shown in Fig. 2c i t can be observed how the Y_2O_3 particles are homogenously distributed

Table 1
Densities of as-cast and sintered samples, expressed as percent of theoretical density.

	Green		Sintered	
Sample	HA	HA10Y	HA	HA10Y
Density (% th)	59	63	68	64

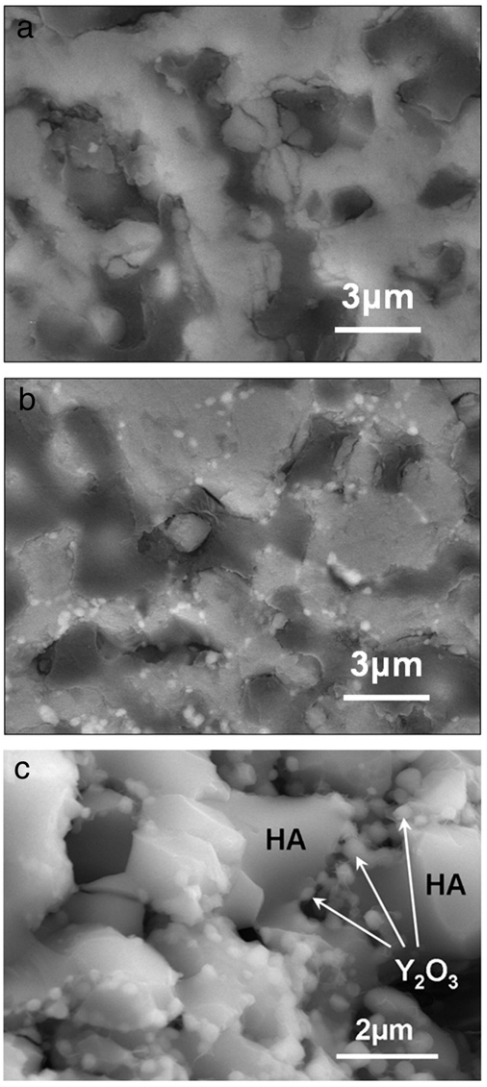

Fig. 2. FE-SEM images of the polished surfaces of sintered (a) HA and (b) HA10Y. Areas with black and dark grey contrast correspond with pore space filled up with epoxy resin. (c) Fracture surface image of the HA10Y sintered composite showing the dispersion of submicrometric Y_2O_3 particles.

coating the HA ones. Since the shrinkage of HA10Y upon sintering is in significant, this particle dispersion appears to inhibit the densification process and shrinkage of the sample [34]. In contrast, the HA10Y material in Ref. [16] did not exhibit such a fine dispersion of particles but large Y_2O_3 agglomerates.

3.2.2. Thermal analysis

Fig. 3 shows the curves of TGA and DTA on green compacts of HA and HA10Y heated from room temperature to 1450 °C.

It can be observed that an evident mass loss occurs between 20 and 400 °C for HA (~0.75%) and HA10Y (~0.50%), which is followed by a plateau for both materials. Above ~600°C HA starts to loss mass again, first slowly up to ~1100 °C, where the rate of mass loss steeply increases up to attaining a maximum rate at ~1350 °C. On increasing temperature above 1400 °C the mass of HA remains constant after having lost about 2.4% of the starting mass. For HA10Y the second stage of mass loss starts at ~900°C with a rate increasing continuously up to get 1.8% mass loss at 1450 °C, which is significantly lower than the corresponding one for HA.

DTA curve of HA shows a broad exothermic peak centered at 350 °C and another weak exothermic peak at 1420 °C. Both peaks are not

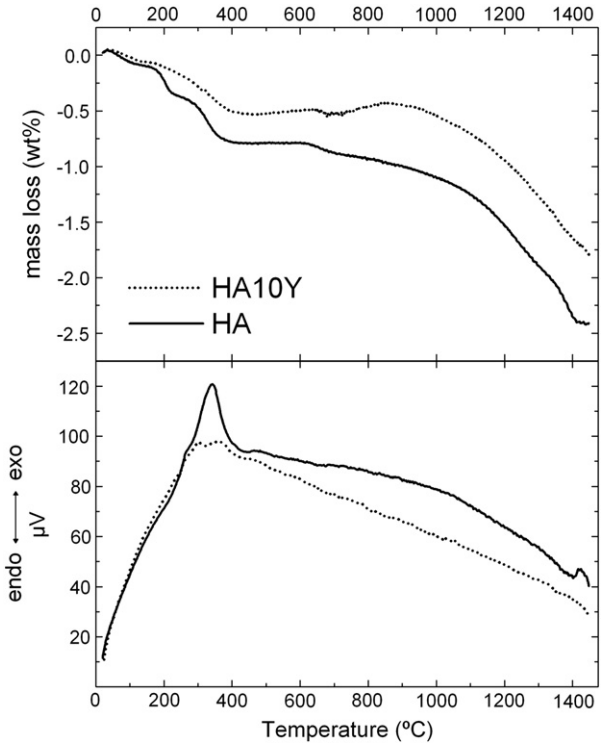

Fig. 3. TGA (upper graph) and DTA (lower graph) curves of HA and HA10Y green powdered samples.

present in the DTA curve of HA10Y. No meaningful exothermic or endothermic peaks were observed.

The initial mass loss up to ~400°C is attributed to the removal of water adsorbed in the surface and pores (up to 200 °C) [1,35] and the loss of lattice water in the rage 200 400 °C. In the case of HA this mass loss is accompanied by a broad exothermic peak centered at ~350 °C in the DTA curve, which is attributed to burning of the residual dispersant present in the green compact.

The second mass loss stage, starting above ~600°C in HA and at ~900 °C in HA10Y, is attributed to progressive dehydroxylation, in agreement with other results reported for different types of HA [1,6,35]. Since the onset temperature of the HA dehydroxylation is shifted by the processing conditions, such as: preparation method of the starting powder, impurities, sintering atmosphere and heating rate, and the Y_2O_3 addition is just the processing parameter distinguishing the HA10Y compacts from the HA ones, the shift of the dehydroxylation to ~900°C is tentatively attributed to the Y_2O_3 addition.

Since Y_2O_3 added to HA appears to raise the density of the green compacts, i.e. it reduces the porosity of the green compacts, it results in less amount of adsorbed water in pores. Therefore a smaller mass loss would be expected in HA10Y during heating at temperatures <400 °C. The increase of mass that can be observed in the HA10Y TGA curve at ~600°C is associated to the in situ rehydration of the dehydrated sample [36]. The higher mass loss observed for HA at ~1150 °C is related to the water release produced by the transformation of HA to β tricalcium phosphate (β TCP) according to the reaction [37,38]:

$$Ca_{10}(PO_4)_6(OH)_2 \rightarrow 3Ca(PO_4) + CaO + H_2O\uparrow \quad (1)$$

Lastly, further mass loss in HA occurs between 1350 and 1400 °C, followed by a plateau with a corresponding exothermic peak in the DTA curve. This significant loss of relative mass in this temperature range, which has also been reported by other authors in HA [6], may be attributed to HA decomposition into α TCP and tetracalcium phosphate (TTCP), $Ca_4P_2O_9$, accompanied by dehydroxylation [39]. According to the idea proposed by Liao et al. [6], the dehydration of HA compacts would not be completely accomplished before decomposition into α TCP and TTCP through the temperature range 1350 1400 °C, and some OA might exist upon HA dehydration at T ≤ 1400 °C. Then, the little exothermic peak observed just above 1400 °C may be due to the decomposition reaction of residual OA into α TCP and TTCP without mass loss, i.e.

$$Ca_{10}(PO_4)_6O\square \rightarrow 2Ca_3(PO_4)_2 + Ca_4P_2O_9 \quad (2)$$

It is evident from the TGA and DTA curves that the addition of Y_2O_3 inhibits the decomposition mechanisms of HA into calcium phosphates, at least up to 1450 °C, but not the HA dehydration. This would allow to control the HA decomposition, increase the processing temperature, and improve the mechanical properties.

3.2.3. XRD and FTIR measurements

To verify the effect of the decomposition mechanisms on the crystallographic structures and the chemical bonding, XRD and FTIR measurements were performed for both HA and HA10Y.

The experimental XRD patterns of HA and HA10Y samples sintered at 1250 °C are presented in Fig. 4, along with the theoretical position of the characteristic diffraction peaks of the phases detected in the samples. These patterns were fitted by FULLPROF. The values of reliability factors of the fit are: R_{wp}=1.8 for HA and R_{wp}=2.7 for HA10Y. Two phases were identified in HA after being sintered: hexagonal HA and β TCP. However, only the presence of hexagonal HA was detected for the HA10Y sample. These results agree with the previous results [16,31,37], and highlight that the addition of Y_2O_3 stabilizes the apatite structure restraining the mechanisms of HA decomposition in β TCP irrespective of whether the processing route is colloidal or dry CIP and sintering as in Ref. [16]. Moreover, these XRD results support the above interpretation of the TGA and DTA results.

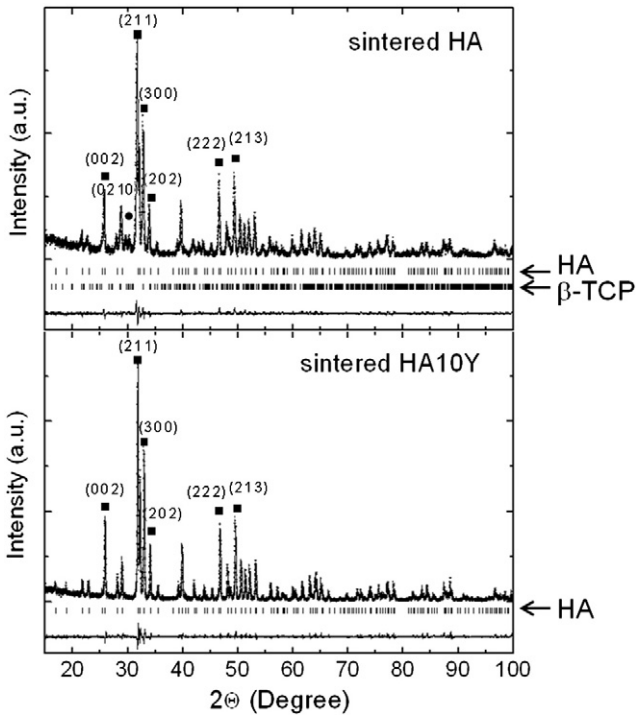

Fig. 4. XRD patterns fitted by FULLPROF for HA and HA10Y samples sintered at 1250 °C. The segments marked at the bottom of each pattern indicate the theoretical positions of the diffraction peaks corresponding to the phases detected in the samples. The lowest trace in each graph represents the deviation of the XRD adjusted patterns from the experimental one. The main peaks for the HA (■) and β-TCP (●) phases are labeled with Miller indices (hkl).

Changes in c and a axis lattice parameters were found from analyses of the HA and HA10Y patterns. The obtained values were: $c_{HA} = 6.90 \pm 0.02$ Å against $c_{HA10Y} = 6.866 \pm 0.005$ Å, and $a_{HA} = 9.44 \pm 0.02$ Å against $a_{HA10Y} = 9.392 \pm 0.004$ Å. The less accurate values measured for pure HA are related to less intense XRD peaks. The apatite cell volume decreases if Y^{3+} ions are dissolved into the HA lattice substituting Ca^{2+}, as expected, because of the size difference of their ionic radii [31].

Fig. 5 shows the FTIR spectra of HA and HA10Y sintered at 1250 °C. The stretching band at 3571 cm^{-1} and vibrational band at 635 cm^{-1} corresponding to OH^- groups, as well as the absorption bands in the range 962 1100 cm^{-1} corresponding to the vibration modes of PO_4^{3-} groups are clearly visible for both materials [31,40,41]. Moreover, a peak at 668 cm^{-1}, attributed to the stretching frequency of a Y O bond, is observed in the spectrum of HA10Y [42]. The comparison between FTIR spectra for HA and HA10Y sintered samples shows that the intensities of the OH^- bands at 3571 cm^{-1} and 635 cm^{-1} in the HA10Y spectrum are lower than the corresponding ones for HA. These results are attribut ed to the substitution of Ca^{2+} by Y^{3+} and charge compensation by an increase of negative charge produced by the transformation of OH^- into $O^{2-\square}$ ion vacancy pairs, and subsequent formation of oxyhydroxyapatite in the form $Ca_{10-y}Y_y(PO_4)_6O_y(OH)_{1-y}\square_y$ with a large number of anionic vacancies in its structure [3,31]. On the other hand, the presence of the strong absorption due to OH^- groups in sintered HA indicates that complete dehydroxylation of HA did not occur at a sintering temperature of 1250 °C.

It is worthwhile to notice that a high ionic conductivity appears to enhance the electrical induced osteoconductivity and osseointegration of HA implants [43 45], which is favored by the presence of anion va cancies in the HA lattice [31,46,47]. Then, it is expected that the addition of Y_2O_3 to HA improves osteoblast adhesion and bone bonding to the HA implants besides increasing its thermal stability and improving other properties related with the processing conditions such as the elastic constants, mechanical strength and microhardness.

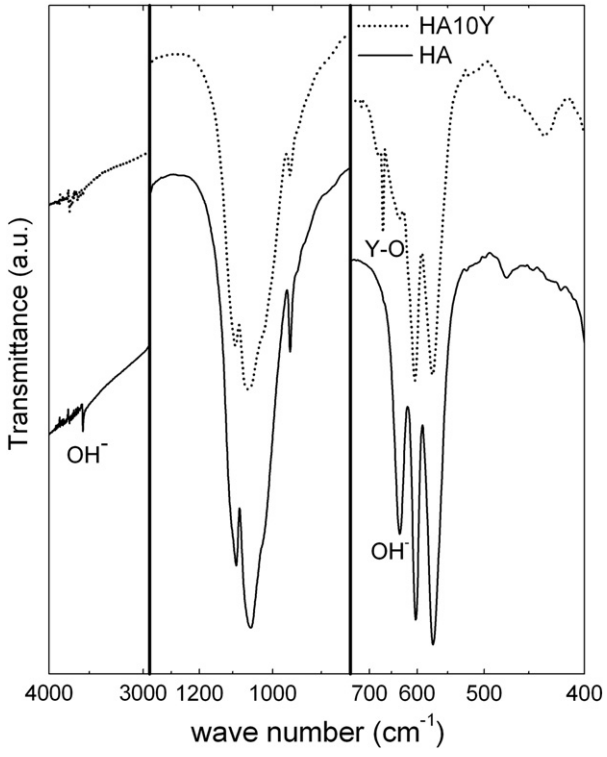

Fig. 5. FTIR spectra of HA and HA10Y sintered at 1250 °C.

4. Conclusions

A highly dispersed 10 wt.% Y_2O_3 hydroxyapatite composite has been fabricated by a colloidal route optimizing the zeta potential values of the starting powders in aqueous suspensions. It has been shown that Y_2O_3 influences the sintering behavior in several ways: (1) restraining grain boundary migration, and consequently maintaining the open porous structure, (2) shifting the onset of the HA dehydroxylation and (3) inhibiting the decomposition into calcium phosphates at tempera tures ≤1450°C.

Then, the addition of Y_2O_3 allows controlling the decomposition mechanisms to take advantage of the inhibition of a calcium phosphate phase, maintaining the densification of the material. Both aspects could be favorable for enhancing the properties of the HA based implantable devices with designed porosity and functional properties.

Acknowledgements

This work has been supported by the Ministry of Science and Innova tion of Spain (MICINN) under contracts MAT2009 14448 C02 01 and IPT 310000 2010 12, and Regional Government of Madrid through the ESTRUMAT CM program (MAT 1585).

References

[1] T. Wang, A. Dorner-Relsel, E. Muller, J. Eur. Ceram. Soc. 24 (2004) 693–698.
[2] J. Cihlar, A. Buchal, M. Trunec, J. Mater. Sci. 34 (1999) 6121–6131.
[3] A. Serret, M.V. Cabanas, M. Vallet-Regi, Chem. Mater. 12 (2000) 3836–3841.
[4] K.A. Gross, C.C. Berndt, P. Stephens, R. Dinnebier, J. Mater. Sci. 33 (1998) 3985–3991.
[5] J.M. Zhou, X.D. Zhang, J.Y. Chen, S.X. Zeng, K. Degroot, J. Mater. Sci. Mater. Med. 4 (1993) 83–85.
[6] C.J. Liao, F.H. Lin, K.S. Chen, J.S. Sun, Biomaterials 20 (1999) 1807–1813.
[7] J. Cihlar, M. Trunec, Biomaterials 17 (1996) 1905–1911.
[8] R.Z. LeGeros, J.P. LeGeros, Y. Kim, R. Kijkowska, R. Zheng, C. Bautista, et al., in: G. Fischman, A. Clare, L.L. Hench (Eds.), Bioceramics: Materials and Applications, American Ceramic Society, Ohio, 1995, p. 173.
[9] R.Z. Legeros, Clin. Mater. 14 (1993) 65–88.
[10] P.N. de Aza, S. de Aza, in: R. Sastre Muñoz, S. de Aza, J. San Román (Eds.), Biomateriales, Faenza Editrice Ibérica S.L., Castellón, 2004, pp. 41–64.
[11] D. Laurencin, N. Almora-Barrios, N.H. de Leeuw, C. Gervais, C. Bonhomme, F. Mauri, et al., Biomaterials 32 (2011) 1826–1837.
[12] P.J. Panteix, I. Julien, P. Abelard, D. Bernache-Assollant, J. Eur. Ceram. Soc. 28 (2008) 821–828.
[13] M. Sato, M.A. Sambito, A. Aslani, N.M. Kalkhoran, E.B. Slamovich, T.J. Webster, Biomaterials 27 (2006) 2358–2369.
[14] J. Al-Haidary, M. Al-Haidari, S. Qrunfuleh, Biomed. Mater. 3 (2008) 015005.
[15] O. Gunduz, S. Daglilar, S. Salman, N. Ekren, S. Agathopoulos, F.N. Oktar, J. Compos. Mater. 42 (2008) 1281–1287.
[16] M.A. Auger, B. Savoini, A. Munoz, T. Leguey, M.A. Monge, R. Pareja, et al., Ceram. Int. 35 (2009) 2373–2380.
[17] S. Nath, N. Sinha, B. Basu, Ceram. Int. 34 (2008) 1509–1520.
[18] R.G. Luthardta, M.S. Holzhutera, H. Rudolpha, V. Herold, M.H. Walter, Dent. Mater. 20 (2004) 655–662.
[19] J. Chevalier, Biomaterials 27 (2006) 535–543.
[20] A. Costantini, R. Fresa, A. Buri, F. Branda, Biomaterials 18 (1997) 453–458.
[21] K.A. Khalil, S.W. Kim, H.Y. Kim, Mater. Sci. Eng., A 456 (2007) 368–372.
[22] M.M. Aydin, L.S. Ozyegin, F.N. Oktar, E.Z. Erkmen, O. Anzabi, K. Gross, Key Eng. Mater. 309–311 (2006) 631–634.
[23] A.J. Sanchez-Herencia, Key Eng. Mater. 333 (2007) 39–48.
[24] F.F. Lange, J. Am. Ceram. Soc. 72 (1989) 3–15.
[25] R.R. Rao, T.S. Kannan, J. Am. Ceram. Soc. 84 (2001) 1710–1716.
[26] J.A. Lewis, J. Am. Ceram. Soc. 83 (2000) 2341–2359.
[27] I. Gonzalo-Juan, B. Ferrari, M.T. Colomer, A.J. Sánchez-Herencia, J. Membr. Sci. 352 (2010) 55–62.
[28] A.J. Sanchez-Herencia, N. Hernandez, R. Moreno, J. Am. Ceram. Soc. 89 (2006) 1890–1896.
[29] L.A. Cyster, D.M. Grant, S.M. Howdle, F.R. Rose, D.J. Irvine, D. Freeman, et al., Biomaterials 26 (2005) 697–702.
[30] P. Parente, O. Burgos, M.A. Auger, M.A. Monge, A.J. Sánchez-Herencia, in: A.J. Sánchez-Herencia, B. Ferrari (Eds.), Book of Abstract for the 4th International Conference on Shaping of Advanced Ceramics (Shaping IV), CSIC, Madrid, 2009, pp. SC1–SC10.
[31] K. Yamashita, H. Owada, H. Nakagawa, T. Umegaki, T. Kanazawa, J. Am. Ceram. Soc. 69 (1986) 590–594.
[32] H.M. Rietveld, J. Appl. Crystallogr. 2 (1969) 65–71.
[33] J. Rodriguez-Carvajal, Physica B 192 (1993) 55–69.
[34] H.Y. Yang, S.F. Yang, X.P. Chi, J.R. Evans, I. Thompson, R.J. Cook, et al., J. Eur. Ceram. Soc. 28 (2008) 159–167.

[35] S.J. Kalita, S. Verma, Mater. Sci. Eng. C Mater. Biol. Appl. 30 (2010) 295–303.
[36] P. Alberius-Henning, E. Adolfsson, J. Grins, A. Fitch, J. Mater. Sci. 36 (2001) 663–668.
[37] S.P. Parthiban, K. Elayaraja, E.K. Girija, Y. Yokogawa, R. Kesavamoorthy, M. Palanichamy, et al., J. Mater. Sci. Mater. Med. 20 (2009) 77–83.
[38] P.N. Kumta, C. Sfeir, D.H. Lee, D. Olton, D. Choi, Acta Biomater. 1 (2005) 65–83.
[39] P.V. Riboud, Ann. Chim. 8 (1973) 381–390.
[40] A. Rapacz-Kmita, A. Slosarczyk, Z. Paszkiewicz, C. Paluszkiewicz, J. Mol. Struct. 704 (2004) 333–340.
[41] A. Slosarczyk, C. Paluszkiewicz, M. Gawlicki, Z. Paszkiewicz, Ceram. Int. 23 (1997) 297–304.
[42] R. Srinivasan, R. Yogamalar, A.C. Bose, Mater. Res. Bull. 45 (2010) 1165–1170.
[43] T. Kobayashi, S. Nakamura, K. Yamashita, J. Biomed. Mater. Res. 57 (2001) 477–484.
[44] B.M. Isaacson, R.D. Bloebaum, J. Biomed. Mater. Res. A 95 (2010) 1270–1279.
[45] M.B. Isaacson, L.B. Brunker, A.A. Brown, J.P. Beck, G.L. Burns, R.D. Bloebaum, J. Biomed. Mater. Res. B 97 (2011) 190–200.
[46] K. Yamashita, H. Owada, T. Umegaki, T. Kanazawa, T. Futagami, Solid State Ionics 28–30 (1988) 660–663.
[47] K. Yamashita, H. Owada, T. Umegaki, T. Kanazawa, Solid State Ionics 40–41 (1990) 918–921.